Offshore Transport of Shelf Waters through Interaction of Vortices with a Shelfbreak Current

CLAUDIA CENEDESE, ROBERT E. TODD, GLEN G. GAWARKIEWICZ, AND W. BRECHNER OWENS

Woods Hole Oceanographic Institution, Woods Hole, Massachusetts

ANDREY Y. SHCHERBINA

Applied Physics Laboratory, University of Washington, Seattle, Washington

(Manuscript received 13 August 2012, in final form 20 December 2012)

ABSTRACT

Interactions between vortices and a shelfbreak current are investigated, with particular attention to the exchange of waters between the continental shelf and slope. The nonlinear, three-dimensional interaction between an anticyclonic vortex and the shelfbreak current is studied in the laboratory while varying the ratio ϵ of the maximum azimuthal velocity in the vortex to the maximum alongshelf velocity in the shelfbreak current. Strong interactions between the shelfbreak current and the vortex are observed when $\epsilon > 1$; weak interactions are found when $\epsilon < 1$. When the anticyclonic vortex comes in contact with the shelfbreak front during a strong interaction, a streamer of shelf water is drawn offshore and wraps anticyclonically around the vortex. Measurements of the offshore transport and identification of the particle trajectories in the shelfbreak current drawn offshore from the vortex allow quantification of the fraction of the shelfbreak current that is deflected onto the slope; this fraction increases for increasing values of ϵ. Experimental results in the laboratory are strikingly similar to results obtained from observations in the Middle Atlantic Bight (MAB); after proper scaling, measurements of offshore transport and offshore displacement of shelf water for vortices in the MAB that span a range of values of ϵ agree well with laboratory predictions.

1. Introduction

Shelfbreak fronts occur along many continental shelves, such as the northwest Atlantic (Wright and Parker 1976), the Celtic Sea (Pingree et al. 1982), and the southeast Bering Sea (Coachman 1986). These fronts typically separate cool, fresh continental shelf waters from warmer, saltier slope waters and are dynamically trapped along the shelf break where the bottom slope suddenly changes (Gawarkiewicz and Chapman 1992). Shelfbreak fronts are robust features that act as barriers between two water masses and are of considerable importance when considering the exchange of water masses and properties between the shelf and slope regions. Exchange of heat, salt, carbon, nutrients, sediments, and other water characteristics between the shelf and slope waters must occur across the shelfbreak front. The residence time in shelf waters and the ultimate fate of pollutants discharged into the coastal zone also depend upon the rate of seaward transport across the front. Episodic offshore transport due to the interaction of vortices with the shelfbreak current can account for a substantial portion of net cross-frontal exchange (Bisagni 1983; Garfield and Evans 1987; Chaudhuri et al. 2009). The offshore transport occurs in shelf water streamers—long filaments of shelf water wrapping anticyclonically around the vortices (Garfield and Evans 1987). Shelfbreak fronts are also regions of enhanced biological activity (Marra et al. 1990; Orphanides and Magnusson 2007) and, as suggested in a model by Flierl and Wroblewski (1985), vortex–current interactions may substantially impact the recruitment of commercially important fish, whose larvae can be caught in shelf water streamers.

A well-studied example of a shelfbreak current system is in the Middle Atlantic Bight (MAB) between Georges Bank and Cape Hatteras, where the shelfbreak front separates warm, salty waters of the North Atlantic Ocean

Corresponding author address: Claudia Cenedese, Woods Hole Oceanographic Institution, 360 Woods Hole Rd., Woods Hole, MA 02543.
E-mail: ccenedese@whoi.edu

DOI: 10.1175/JPO-D-12-0150.1

from cooler, fresher subarctic waters over the continental shelf (Wright and Parker 1976; Linder and Gawarkiewicz 1998). Farther offshore, meanders of the Gulf Stream pinch off to form anticyclonic mesoscale vortices that contain warm, salty water from the Sargasso Sea in their cores. These vortices are referred to as warm core rings (WCRs) and often impinge upon the shelfbreak current, pulling shelf water offshore and forcing on-shelf intrusions of WCR water or along-shelf currents (e.g., Evans et al. 1985; Wei et al. 2008). However, strong vorticity constraints due to the steep topography over the upper slope prevent the central portion of WCRs (with solid body rotation) from extending shoreward of the shelf break onto the continental shelf. Observational programs have investigated some aspects of the importance of mesoscale vortices to the cross-frontal exchange of water proprieties in the MAB (e.g., Churchill et al. 1986; Garfield and Evans 1987; Joyce et al. 1992; Chaudhuri et al. 2009) and the impact of WCRs on the shelfbreak frontal structure (Gawarkiewicz et al. 2001), but we still lack a complete understanding of the dynamics because of the complexity introduced by nonlinearity and three-dimensionality.

In the MAB, remote sensing of sea surface temperatures (SSTs) shows the regular formation of streamers as WCRs approach the MAB shelf break (e.g., Fig. 1b); cooler shelf water is pulled offshore on the eastern side of the WCR. Seven years of SST imagery and concurrent ship-based observations revealed that an average of seven rings per year were located south of the Georges Bank region during the period 1979 through 1985 and that streamers occurred approximately 70% of the time (Garfield and Evans 1987). Estimates of instantaneous streamer transport vary over an order of magnitude (Morgan and Bishop 1977; Smith 1978; Bisagni 1983; Wei et al. 2008), much of which is attributable to natural variability (Garfield and Evans 1987). Chaudhuri et al. (2009) estimate that the annual average offshore transport due to streamers in the MAB is 0.13 Sv (1 Sv $\equiv 1 \times 10^6$ m^3 s^{-1}), an estimate that accounts for more than one-third of the total offshore transport of 0.35 Sv based on a Gulf of Maine volume transport box model (Loder et al. 1998). Tang et al. (1985) and Churchill et al. (1986) found that shelf water streamers do not always have a surface signature, and the three-dimensional subsurface streamers could represent a significant term in the mass budget. Furthermore, rather than drawing shelf water from inshore of the shelfbreak front offshore, the water forming a streamer may originate only in the outer edge of the shelfbreak front (Brink et al. 2003).

Interactions between vortices and shelfbreak frontal systems are also important in a number of other geographical settings. A few examples include the Bering Sea Green Belt (Springer et al. 1996), the southwest Atlantic shelf east of Argentina (Bogazzi et al. 2005), and the Black Sea (Oguz et al. 1993). In each of these regions, enhanced biological productivity occurs near

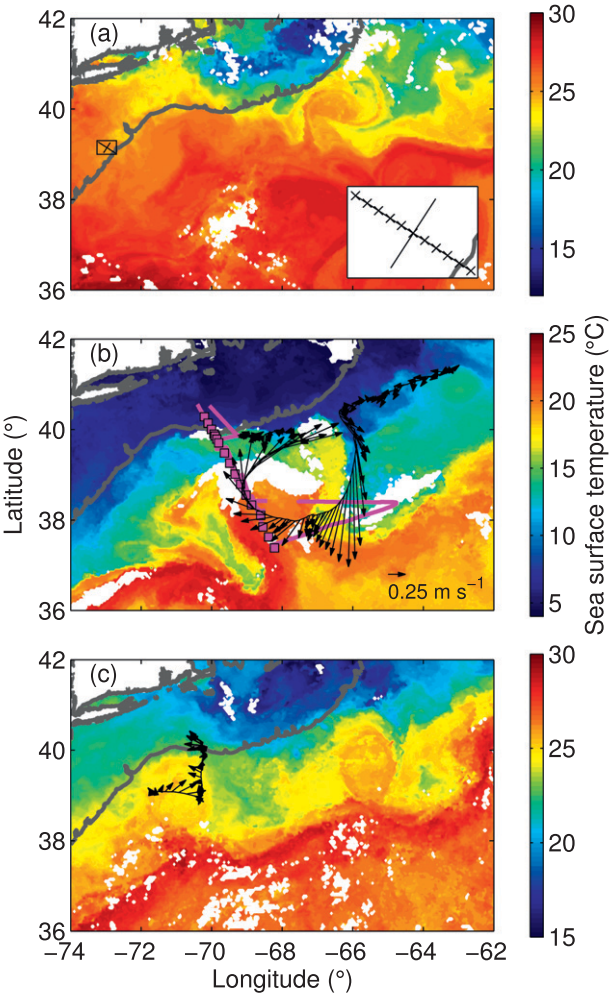

FIG. 1. Average SSTs over the MAB shelf break and slope during (a) 21 Jul 2005, (b) 27 Mar–1 Apr 2006, and (c) 28 Aug–3 Sep 2007 from the Moderate Resolution Imaging Spectroradiometer (MODIS) sensors aboard the *Terra* and *Aqua* satellites. Note that the color scales vary between panels. White patches represent missing data, primarily because of cloud coverage. In (a), the tracks of the REMUS AUV on 21 Jul and R/V *Tioga* on 24 Jul are shown inside the boxed region near 39°N, 73°W; this region is expanded in the inset map where R/V *Tioga* stations are shown by ×'s. In (a), the streamer and associated anticyclone are not apparent in the SST imagery because of warm surface temperatures throughout the region at the height of summer. In (b),(c), vertically averaged currents measured along the track of the Spray gliders are shown for the periods 15 Mar–15 Apr 2006 and 28 Aug–9 Sep 2007, respectively (black vectors). In (b), locations of ship-based hydrographic stations along Line W and shipboard ADCP measurements during April 2006 are shown by the magenta squares and line, respectively. The coastline and 200-m isobath (i.e., the shelf break) are drawn in gray.

the shelf break, and understanding the impact of vortices on both the circulation and the ecosystem dynamics is important.

It is clear that the interaction of a vortex with a shelfbreak front is a complicated, three-dimensional, nonlinear problem, and basic questions about processes controlling the cross-frontal exchange remain largely unanswered. How much shelf water moves offshore through streamers? Where does the water within the streamers originate on the continental shelf? How far offshore is the streamer's water transported? Does the slope water actually cross onto the continental shelf to replace the water withdrawn by the vortex? What is the fate of the vortex after encountering the shelfbreak front? This study attempts to answer these questions using idealized laboratory experiments and oceanographic observations. The paper is organized as follows: the experimental apparatus is described in section 2a while the oceanic observations are described in section 2b; experimental results describing the interaction between an anticyclonic vortex and a shelfbreak current are presented and discussed in sections 3a and 3b and compared to the oceanic observations in section 3c; a summary and conclusions are presented in section 4; and the appendix discusses the interaction of cyclonic vortices with a shelfbreak current.

2. Methods

a. Experimental apparatus

The experiments are conducted in a 30-cm deep transparent Perspex (acrylic glass) tank with a circular base of radius $R = 57.5$ cm mounted concentrically on a 2-m diameter, rotating table with a vertical axis of rotation (Fig. 2). The shelfbreak current is generated against a vertical boundary formed by a Perspex cylinder of radius $R_0 = 13$ cm, also concentric with the axis of rotation so that the flow is confined in an annular region 44.5 cm wide. As in Cenedese and Linden (2002), the shelfbreak geometry is simulated by the walls of a truncated cone positioned in the middle of the tank (Fig. 2). Hereafter, we will refer to the flat region of width $W = 7$ cm over the top of the truncated cone as the shelf, the edge of the flat region as the shelf break, and the sloping wall of the cone as the slope. The slope of the truncated cone is given by $s^* = \tan\alpha^* = 22$, where $\alpha^* = 87.4°$ is the angle between the slope and the horizontal.

The tank is filled with a salt solution of density ρ_a to a maximum fluid depth at the tank wall H, and is brought to solid body rotation. The shelfbreak current is generated by releasing a constant volume of dyed fluid of density $\rho_c < \rho_a$ from a circular source positioned at the free surface around the inner Perspex cylinder. The entire volume is released before the vortex is generated. The source consists of a ring of copper tubing containing many small holes, covered with plastic foam, and positioned at the free surface, adjacent to the cylindrical boundary. This source fits snugly around the inner cylinder and introduces the surface buoyant fluid almost uniformly around the circumference of the cylinder. The volume of buoyant fluid introduced is such that the current is approximately as wide as the shelf (i.e., W) and as deep as the fluid over the shelf (i.e., h_c). To maintain a baroclinically stable current, the width of the current is kept smaller than the Rossby radius of deformation of the current $R_c = \sqrt{g_c' h_c}/f$, where h_c is the depth of the

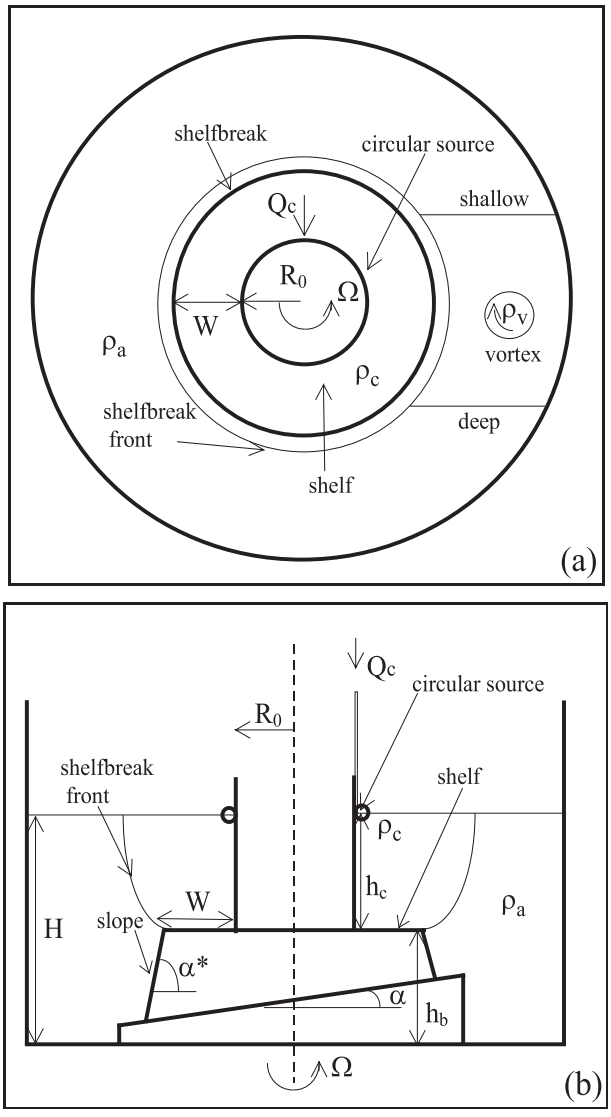

FIG. 2. Sketch of the experimental apparatus: (a) top view, (b) side view. Not to scale.

TABLE 1. Overview of the experimental parameters and measured quantities ordered by increasing values of ϵ.

Expt	ϵ	f (s^{-1})	g_c' (cm s^{-2})	g_v' (cm s^{-2})	h_c (cm)	h_v (cm)	d_{max}/R_c	D_{max}/R_c	T_s/Q
1	0.28	1.5	4.2	0.2	2.0	3.7	0.00	2.86	0.21
2	0.37	2.0	4.2	0.2	1.9	4.7	0.00	4.36	0.27
3	0.58	1.5	2.4	0.4	2.0	3.9	−0.03	4.60	0.11
4	0.66	1.5	4.5	1.0	2.0	4.0	0.56	3.44	0.08
5	0.69	2.0	4.5	1.0	1.9	4.0	−0.19	3.72	0.06
6	0.74	1.5	2.3	0.3	1.0	4.0	0.04	6.93	0.20
7	0.90	1.5	2.4	1.1	2.0	3.5	−0.30	7.18	0.36
8	1.04	1.5	4.4	2.0	1.8	4.3	−0.39	6.61	0.23
9	1.05	2.0	4.4	2.0	1.7	4.0	0.00	7.50	0.20
10	1.13	2.0	4.4	3.0	1.9	3.5	0.59	8.86	0.12
11	1.13	1.5	4.4	3.0	2.0	3.8	−0.08	6.80	0.08
12	1.16	1.5	2.3	2.1	2.0	3.0	0.76	9.57	0.23
13	1.33	1.5	4.2	4.4	2.0	3.4	0.66	7.46	0.09
14	1.35	1.5	2.3	2.9	2.0	2.9	1.16	10.82	0.57
15	1.37	2.0	4.4	4.4	1.9	3.5	0.76	9.14	0.55
16	1.55	1.5	2.2	4.4	2.0	2.4	0.32	11.70	0.73
17	1.68	1.5	2.3	2.0	1.0	3.3	0.20	15.21	0.36
18	1.96	1.5	2.3	3.1	1.0	2.9	0.31	15.44	0.37
19	2.07	1.5	2.3	4.4	1.0	2.3	2.61	15.76	1.72
20	2.11	1.5	2.2	4.4	1.0	2.3	2.67	16.19	1.24

current, $g_c' = g[(\rho_a - \rho_c)/\rho_a]$ is the reduced gravity in the shelfbreak current, g is the gravitational acceleration, Ω is the angular frequency of the rotating table, and $f = 2\Omega$ is the Coriolis parameter (Cenedese and Linden 2002).

After the shelfbreak current has reached steady state, a baroclinic anticyclonic vortex is generated far away from the shelfbreak current (see Fig. 2) by injecting fluid of density $\rho_v < \rho_a$ as in Cenedese and Linden (1999). For most experiments $\rho_c < \rho_v < \rho_a$, but for six experiments $\rho_v < \rho_c < \rho_a$ (Table 1). A sloping bottom with $s = \tan\alpha = 0.5$, where $\alpha = 26.6°$ is the angle between the slope and the horizontal, is positioned between the generation site of the vortex and the truncated cone (Fig. 2) to simulate the planetary β effect. The presence of the sloping bottom simulating the planetary β effect does not influence the shelfbreak frontal structure since the shelfbreak front is positioned above the cone's much steeper sloping wall. The use of a sloping bottom to represent a β plane is strictly valid only for an unstratified fluid. In the 1½-layer stratification used here, the slope provides an equivalent potential vorticity (PV) gradient in the lower layer, but there is not a direct representation of the PV gradient in the upper layer. Nevertheless, the thermal wind coupling across the interface implies that the motion in the upper layer is also influenced by the lower layer PV gradient. Hence, the essential features of a β plane are captured using a slope, where the shallowest part of the tank corresponds to the ''northern'' shore of the Northern Hemisphere topographic β plane. Vortices over a sloping bottom move along isobaths (Nof 1983; Cenedese and Whitehead 2000), and the anticyclonic vortex propagates westward and interacts with the shelfbreak current. As discussed by Cenedese and Whitehead (2000), in order for the vortex to drift westward in the laboratory, the slope s has to be larger than 0.05, the value representative of the planetary $\beta = 1.57 \times 10^{-13}$ cm^{-1} s^{-1} at 45° latitude. The spin down processes present in the laboratory due to bottom friction acting on the anticyclonic vortices require a much larger slope than scaling would suggest.

The buoyancy forces are described by the reduced gravity of the current g_c' and of the vortex $g_v' = g[(\rho_a - \rho_v)/\rho_a]$. In the experiment g_c' takes values between 2.2 and 4.5 cm s^{-2}, g_v' varies between 0.2 and 4.4 cm s^{-2}, and the Coriolis parameter f is either 1.5 or 2.0 s^{-1}. The flowrate through the circular source is held constant at $Q_c = 10$ cm^3 s^{-1} for the time necessary to fill up the volume over the shelf. The depth of the water below the circular source determines the depth of the current h_c, and varies between 1.0 and 2.0 cm (Table 1). The shelfbreak current always extended to the bottom of the shelf region. The flow rate of the fluid generating the vortex Q_v varies between 1.7 cm^3 s^{-1} and 8.6 cm^3 s^{-1}, and it is continuous for a time long enough to generate the vortex; this time depends on the Rossby radius of deformation of the vortex, $R_v = \sqrt{g_v' h_v}/f$, where h_v is the depth of the vortex.

A video camera is mounted above the tank and fixed to the turntable so that velocity measurements are obtained in the rotating frame. To acquire and process the images from the video camera, we use a computer system with a frame-grabber card and the image-processing

software DigImage (Dalziel 1992). The current and the vortex are made visible by dying the source water with food coloring and by adding buoyant paper pellets on the free surface. The motion of the dyed current is observed from both the top and side. The current and vortex depths are determined from side-viewing images. Using the software DigImage, velocities are measured by tracking paper pellets floating on the free surface, a method known as Particle Tracking Velocimetry (PTV, Dalziel 1992). Typically, fewer than 500 paper pellets are located in each frame and the velocities are obtained by sampling the video at a frequency of approximately 2 Hz. Automatic matching of these locations to the ones in previous frames produces the tracking files. Particle velocities are calculated over 5 samples and the velocity field is obtained by mapping the individual velocity vectors onto a rectangular grid using a spatial averaging over 4 cm and time averaging over 1.3 s. The vorticity is calculated from this gridded velocity data. The error in the measured velocities is estimated to be less than 10% (Linden et al. 1995).

The interaction between the anticyclonic vortex and the shelfbreak current can be characterized by three measurable quantities: the cross-shelf origin of the water contained in the streamer d, which determines the water properties in the streamer and its tracer content (e.g., nutrients, sediments, fish larvae); the most offshore destination of the buoyant water in the streamer D, which is related to the likelihood the buoyant water will be permanently exchanged; and the volume transport of the streamer T_s, which quantifies the cross-frontal exchange. As illustrated in Fig. 3, part of the shelfbreak current is pulled offshore by the vortex and wraps around it to form a streamer. Using the particle trajectories, the most onshore trajectory in the shelfbreak current that is deflected offshore by the vortex is identified (black thin line in Fig. 3). Additionally, we identify the location of the maximum velocity in the shelfbreak current using the velocity fields (dotted line in Fig. 3). The radial distance between these two locations defines the parameter d, which is defined positive when the deflected trajectory is inshore of the location of the maximum velocity in the shelfbreak current (as illustrated in Fig. 3). The radial distance between the location of the maximum velocity in the shelfbreak current (dotted line in Fig. 3) and the most offshore trajectory in the streamer defines the parameter D. The schematic in Fig. 3 represents a particular instant of the interaction and the values d and D are time dependent. The interaction period is divided into 10-s intervals, and d and D are measured in each time interval; we then report the maximum values of these parameters, $d_{\max}$ and $D_{\max}$, scaled by the Rossby radius of deformation of the shelfbreak current R_c. Finally, side-viewing

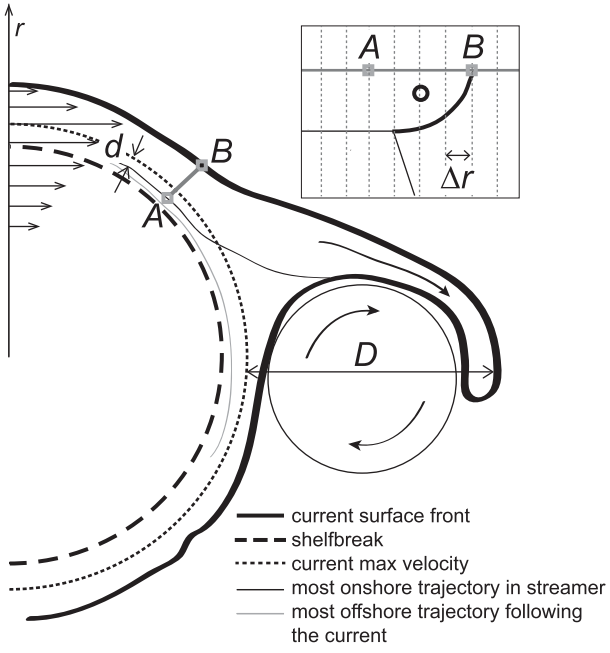

FIG. 3. Sketch illustrating the top view of the interaction between the anticyclonic vortex and the shelfbreak current. Thick solid line denotes the shelfbreak current front. Dashed line denotes the location of the shelf break and dotted line denotes the location of the shelfbreak current maximum velocity prior to the interaction. The two thin lines indicate the trajectories of two particles close to each other upstream of the interaction and then either deflected in the streamer around the vortex or following the shelfbreak current. The locations A and B used for the streamer transport calculation, and the definitions of the parameters D and d are also illustrated. Inset illustrates a radial vertical section through the shelfbreak current and the locations of A and B.

images of the shelfbreak current, together with the surface velocity fields, are used to measure the geostrophic transport of the shelfbreak current, given by $Q = g_c' h_c^2/2f$, and the averaged offshore transport of the streamer T_s. At each location the velocity within the shelfbreak current is assumed to be constant in depth and equal to its surface value. The streamer transport is defined as

$$T_s = \left(\sum_A^B v_i h_{ci} \right) \Delta r, \tag{1}$$

where the subscript i denotes different velocity grid points of horizontal extent Δr (Fig. 3, inset). In the vertical plane where the shelfbreak current depth h_c is measured (using the side digital images), the surface location of the most onshore trajectory in the shelfbreak current that is deflected offshore by the vortex (black thin line in Fig. 3) is denoted by A, and the surface location of the shelfbreak front is denoted by B. The dimensionless parameter T_s/Q gives the streamer transport

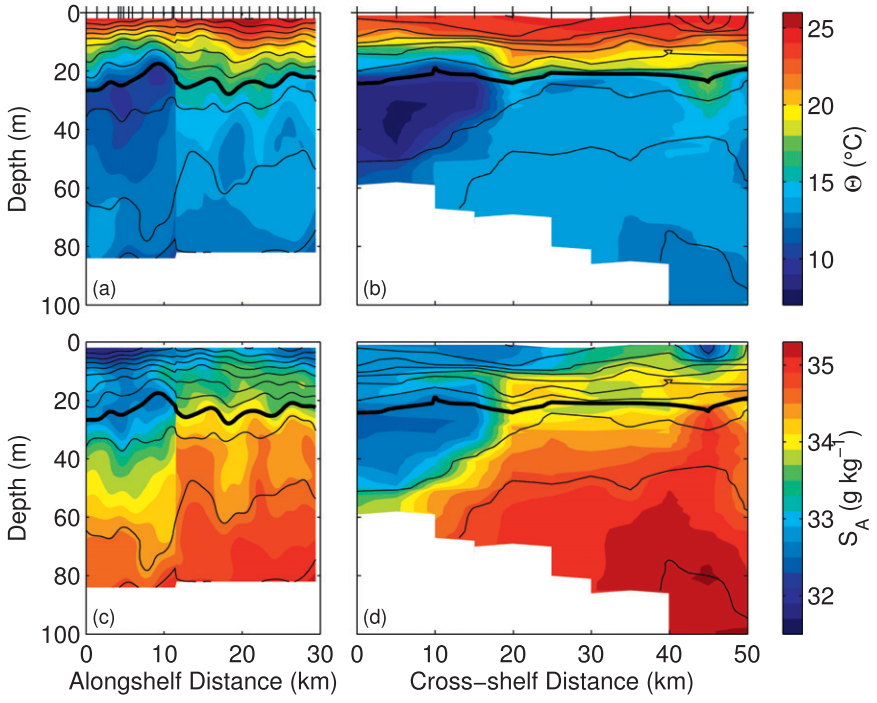

FIG. 4. (a),(c) Along- and (b),(d) cross-shelf hydrographic transects near the shelf break off New Jersey (Fig. 1a). The alongshelf transect was sampled by a REMUS AUV on 21 Jul 2005; the cross-shelf transect was sampled from R/V *Tioga* on 24 Jul 2005. Color contours show (a),(b) Conservative Temperature and (c),(d) Absolute Salinity. Density is denoted by the black contours, with a contour interval of 0.5 kg m^{-3} and the 25.0 kg m^{-3} isopycnal shown bold. The offshore-directed streamer of shelf water is located between 0 and 12 km in (a),(c). The sharp discontinuity at 12 km in the AUV transect is due to a malfunction of the AUV, which surfaced and was redeployed shortly after restarting the vehicle. The tick marks on the upper axis of (a) denote the midpoints of AUV dive cycles, and the tick marks on the upper axis of (b) indicate location of ship-based hydrographic stations. Alongshelf distance increases northeastward and cross-shelf distance increases offshore (southeastward).

as a fraction of the geostrophic transport in the shelfbreak current. The values of the above parameters for each experiment are shown in Table 1.

b. Middle Atlantic Bight observations

Examples of anticyclonic vortices interacting with the shelfbreak front in the Middle Atlantic Bight near Cape Cod are compared to the laboratory experiments. Observations of temperature, salinity, and velocity were collected using a variety of platforms. The observations of vortices interacting with the shelfbreak front used in this study were collected fortuitously; none of the surveys were planned to target anticyclones.

An autonomous underwater vehicle (AUV) was used in July 2005 to study alongshelf variability at the 80-m isobath near the shelf break off New Jersey (Fig. 1a). The Remote Environmental Monitoring Units (REMUS) 100 vehicle was operated in triangle mode, which cycles the vehicle from a depth of 2 m down to a point 2 m above the bottom and back to the near surface. An alongshelf transect, nearly 30 km long, was sampled on 21 July. The transect from the AUV showed evidence of a streamer of shelf water moving offshore with strong alongshelf gradients in temperature, salinity, and density (Figs. 4a,c). On 24 July, hydrographic measurements across the shelfbreak front were made from R/V *Tioga* using traditional vertical casts from the ship (Fig. 4b,d). The cross-shelf transect resolved the shelfbreak front, which was shoreward of its mean climatological position (Linder and Gawarkiewicz 1998).

In the spring of 2006, a large WCR formed from a meander of the Gulf Stream southeast of Cape Cod. From 15 March to 15 April, a Spray glider (Sherman et al. 2001; Rudnick et al. 2004) completed a survey that took it westward along the continental slope until it encountered the WCR and was advected around the ring (Fig. 1b). The glider measured temperature (Fig. 5a), salinity (Fig. 5b), and vertically averaged currents (Fig. 1b, black vectors) over the upper 500–1000 m of the water column. Cross-track geostrophic velocity, referenced to the measured vertically averaged velocities, is

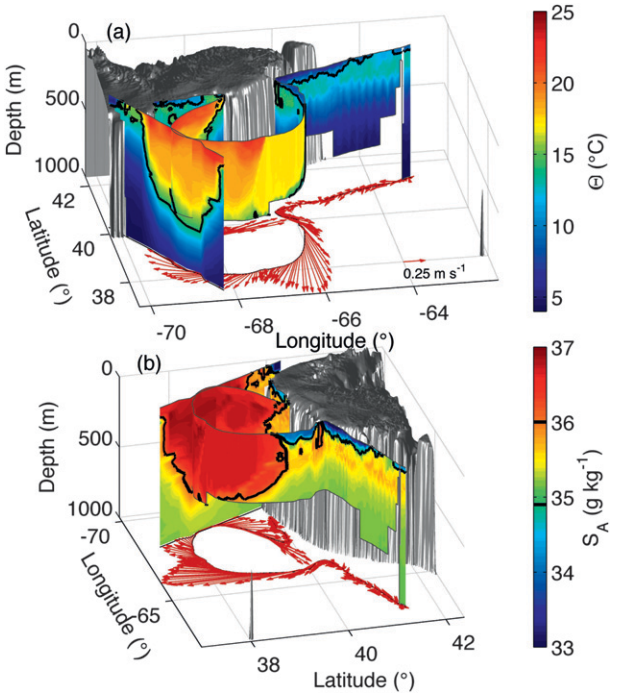

FIG. 5. Hydrographic observations in and near the WCR located offshore of Georges Bank in the spring of 2006 (Fig. 1b). (a) Conservative Temperature Θ and (b) Absolute Salinity S_A shown in color from the glider survey and R/V *Oceanus* survey. Salinity contours of 34.9 and 36.0 g kg^{-1} are drawn black in (a),(b). Note that Θ is shown looking from the south in (a), while S_A is shown looking from the east in (b). Vertically averaged currents (as in Fig. 1b) along the glider's track are represented by the red vectors with a scale vector in the lower right corner of (a). The local bathymetry shallower than 1000 m, which is dominated by Georges Bank, is shown in gray. A portion of a streamer of cold, fresh shelf water is apparent on the eastern side of the WCR.

calculated from objectively mapped horizontal density gradients as in Todd et al. (2011). During 5–15 April, R/V *Oceanus* surveyed in the same area as part of the semiannual occupation of Line W (Toole et al. 2011). Full-depth measurements of temperature and salinity were made at 17 stations (Fig. 1b, magenta squares), and we use observations within the upper 1000 m. Ocean velocity in the upper 500–800 m was measured along the ship track (Fig. 1b, magenta line) with a shipboard acoustic Doppler current profiler (SADCP). The RDI Ocean Surveyor 75-kHz instrument was set to measure in 8-m bins with ensemble averages every 5 min; data processing was performed using the standard University of Hawaii Data Acquisition System (UHDAS) software (see http://currents.soest.hawaii.edu), and an upper bound on absolute accuracy is 0.03–0.05 m s^{-1}. Tidal velocities can be large near the MAB shelf break (Shearman and Lentz 2004), so barotropic tidal currents were removed from the SADCP measurements using Oregon State's TOPEX/Poseidon (TPXO) 7.2 product (see http://volkov.oce.orst.edu/tides/) and Earth and Space Research's Tidal Model Driver toolbox in Matlab (see http://polaris.esr.org/ptm_index.html). To account for the 21-m surface blank in the SADCP data, we simply assumed that the currents were constant from the surface to the shallowest measurement bin; we assume that near-bottom velocities are small and make no correction for the similarly sized data gap near the bottom. The same WCR was also studied using a data-assimilating numerical model (Chen 2011) and was observed to cause exceptionally large anomalies in a time series of mooring observations offshore of the continental shelf (Peña-Molino et al. 2013).

During the summer of 2007, a smaller anticyclonic vortex was located near the continental slope south of Cape Cod (Fig. 1c). From June to October of 2007, a Spray glider was conducting a survey in the region (39°, 40.25°N) × (70.25°, 71.75°W). As in 2006, the glider measured temperature (Fig. 6a), salinity (Fig. 6b), and vertically averaged currents (Fig. 1c), and cross-track geostrophic currents (Fig. 6) are calculated as in Todd et al. (2011). Of the numerous transects completed during the four-month deployment, an alongshelf transect near 39°N from 28 August to 2 September and the subsequent cross-shelf transect along 70.3°W during 2–9 September (Fig. 1c) provide the most useful observations of the anticyclone. This anticyclone was smaller and weaker than expected for a WCR, but it did contain warm, salty waters from the Gulf Stream within its core (Fig. 6). Gaps in the SST record owing to cloud coverage prevent us from determining whether or not the eddy formed from a meander of the Gulf Stream, so we do not refer to it as a WCR.

To the best extent possible, we calculate the same parameters for the vortices observed in the MAB as for the vortices in the laboratory. Velocities for the shelfbreak current v_c and vortices v_v are reported as maximum values; for the glider observations, the larger of the maximum cross-track geostrophic velocity and the maximum vertically averaged velocity magnitude is used. (Since the glider measures both horizontal components of the vertically averaged velocity, the magnitude of the vertically averaged velocity can be larger than the cross-track geostrophic velocity.) In July 2005, the streamer velocity is taken to be a proxy for the maximum vortex velocity as there were no hydrographic measurements made over the continental slope. In spring 2006, the glider did not survey the shelfbreak current, so no estimate of v_c is available from those glider observations, but R/V *Oceanus* did survey the shelfbreak current during that time. In 2007, our estimate of v_c comes from the glider's only crossing of the shelfbreak jet, which

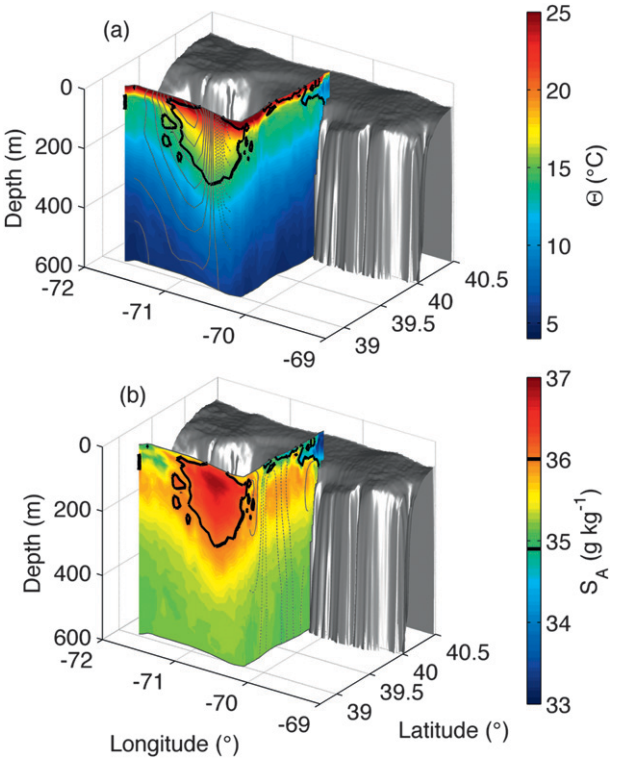

FIG. 6. Hydrographic observations in and near the anticyclonic vortex located south of Cape Cod in the summer of 2007 (Fig. 1c). Contours of across-track geostrophic velocity referenced to measured vertically averaged currents are shown in gray; in (a), northward (solid) and southward (dotted) velocities are shown with a contour interval of 0.05 m s^{-1}. In (b), eastward (solid) and westward (dotted) velocities are shown with the same contour interval. Glider observations of Conservative Temperature Θ and Absolute Salinity S_A are shown in color in (a) and (b), respectively. The bathymetry of the continental shelf and slope are shown in gray.

occurred at the end of the deployment in the latter half of October (see Todd et al. 2013, their Fig. 2). We use Absolute Salinity (Intergovernmental Oceanographic Commission 2010) to differentiate between shelf, slope, and vortex waters; shelf waters have salinities less than 34.9 g kg^{-1}, slope waters have salinities between 34.9 and 36.0 g kg^{-1}, and vortex waters, which originate in the Gulf Stream, have salinities greater than 36.0 g kg^{-1} (Wright and Parker 1976). We define the depths of the shelfbreak current h_c and vortices h_v to be the maximum depths at which shelf or vortex waters are found, respectively. Characteristic densities of the shelf (ρ_c), slope (ρ_a), and vortex (ρ_v) waters are defined as the average surface-referenced potential density for observations in each salinity range. Using the value of f at 40°N (approximately the latitude of the interaction), we calculate the reduced gravities g'_c and g'_v and the Rossby radii of deformation R_c and R_v as for the laboratory experiments. It is not feasible to estimate the parameter d from available observations, but we do estimate D from the farthest offshore (southward) extent of shelf water from the shelf break (taken to be 40°N). Parameters estimated from the various observations are given in Table 2.

Though none of the observations during 2006 and 2007 allow for a direct calculation of the streamer transport, we can estimate the relative offshore transport of shelf waters T_s/Q in spring 2006 in two ways. Based on SADCP measurements in the upper 100 m between 39.75° and 40.5°N during the outbound survey of R/V *Oceanus*, westward transport by the shelfbreak current prior to the interaction with the WCR was 0.29 Sv. When R/V *Oceanus* crossed the shelfbreak front again en route to Woods Hole, transport along the shelf break had reversed and increased in magnitude to 0.39 Sv. The change in transport along the shelf break suggests a net offshore transport by the streamer exceeding twice the shelfbreak current transport ($T_s/Q \approx 2.3$). From the observed depth of shelf waters (h_c, Table 2), glider-measurements of vertically averaged currents within the streamer, and SST imagery (Fig. 1b), we can make a crude estimate of the streamer transport. Taking the width of the streamer to be 25 km and the offshore velocity to be 0.5 m s^{-1}, streamer transport is estimated to be about 1 Sv with a resulting estimate of $T_s/Q \approx 3.4$. Chen (2011) found instantaneous streamer transports as large as 2.1 Sv in their numerical simulation, so this estimate is reasonable.

In 2005, the transport within the shelfbreak front was 0.17 Sv, with a maximum velocity v_c of 0.15 m s^{-1}. The maximum velocity and transport are computed from thermal wind calculations referenced to zero velocity at the bottom and averaged over one baroclinic Rossby radius (5.3 km) in the horizontal to minimize noise from internal waves. In comparison, the streamer transport was 0.086 Sv, with a maximum velocity of 0.22 m s^{-1}. Estimates of reduced gravity and the size of the baroclinic Rossby radius based on the alongshelf density difference measured by the REMUS AUV appear in Table 2.

3. Results and discussion

The interaction of a self-propagating, baroclinic, anticyclonic vortex with a shelfbreak current can be classified as "weak" or "strong." The classification into two distinctive regimes is somewhat arbitrary since a smooth and continuous transition is observed between the two regimes. However, for clarity and simplicity, we use a binary classification. The strength of the interaction is controlled by the relative intensity of the vortex and the shelfbreak current, so we define the parameter ϵ to be the ratio of the maximum azimuthal velocity in the vortex to

TABLE 2. Parameters for anticyclonic vortices in the MAB.

Data source	v_c (m s^{-1})	v_v (m s^{-1})	ϵ	h_c (m)	h_v (m)	g'_c (m s^{-2})	g'_v (m s^{-2})	R_c (km)	R_v (km)	$\frac{D_{\max}}{R_c}$	$\frac{T_s}{Q}$
2005 AUV	0.15	0.22	1.47	84	—	0.003	—	5	—	—	0.5
2006 Glider	—	1.32[a]	—	110	600[b]	0.009	0.007	10	22	6.6	—
2006 Line W	0.45	1.95	4.33	80	680	0.014	0.010	11	28	—	2.3–3.4
2007 Glider	0.55[c]	0.48[c]	0.86	120	250	0.019	0.012	16	18	6.3	0[d]

[a] Maximum observed vertically averaged current magnitude.
[b] Eddy water present at maximum profiling depth.
[c] Maximum cross-track geostrophic velocity.
[d] No clear indication of streamer formation.

the maximum alongshelf velocity in the shelfbreak current. A strong (weak) interaction is characterized by a large (small) value of ϵ, and $\epsilon = 1$ characterizes the transition between weak and strong interactions.

In the laboratory, the shelfbreak current is generated over the shelf and, although its width is less than R_c, develops some meanders. Figures 7a and 8a show the wavelike disturbance at the density front over the shelf break. Initially, the meandering of the shelfbreak current generates anticyclonic disturbances. However, cyclonic relative vorticity, initially concentrated at the outer edge of the current, moves behind the crests of the waves and produces regions of cyclonic motion at the troughs. The cyclonic vortices entrain fluid from the waves, which break ''backward'' relative to the direction of the current. Such disturbances do not grow to large amplitude as observed in previous studies by Griffiths and Linden (1981) and Cenedese and Linden (2002). Thus these meanders are confined to the shelfbreak region and are not responsible for transporting shelf water offshore.

a. *Weak interactions* ($\epsilon < 1$)

After the self-propagating anticyclonic vortex starts interacting with the shelfbreak current, the vortex fluid is pulled away from the vortex by the shelfbreak current in a manner similar to the way that thread unwinds from a spool. After leaving the vortex, the fluid follows the shelfbreak current and occupies the outermost part of the shelfbreak front, as shown by the red trajectories of ''synthetic drifters'' released in the vortex at $t = 1.3T$ (where T is the rotation period, and $t = 0$ when the anticyclonic vortex generation is completed) and advected using the velocity fields obtained by particle tracking (Fig. 7b, red trajectories). The trajectories of synthetic drifters released in the shelfbreak current upstream of the interaction region at $t = 1.3T$ (Fig. 7b, blue trajectories) show that the meanders of the shelfbreak current are slightly deflected by the presence of the vortex, move over it, and reconnect with the current downstream of the region in which the interaction occurred. For the experiments in which $\epsilon < 1$, the vortex water is engulfed by the shelfbreak current, and the buoyant shelf water is only deflected slightly offshore and reconnects to the shelfbreak current downstream of the interaction region. No permanent loss of fluid from the shelf to the offshore is observed.

Measurements from the various experiments with $\epsilon < 1$ confirm the qualitative observations for weak interactions. The parameter $d_{\max}/R_c$ identifies the source of buoyant shelf water contained within a streamer (Fig. 3) and its dependence on ϵ is shown in Fig. 9. For $\epsilon \lesssim 1$, only the buoyant fluid in the proximity of the shelfbreak front where the velocity is maximum is affected by the interaction; that is, $d_{\max}/R_c \approx 0$. For the two experiments with the smallest values of ϵ, streamer formation is not observed, and we arbitrarily assign $d_{\max}/R_c = 0$. For three experiments having $\epsilon < 1$ the value of $d_{\max}/R_c$ is negative, indicating that only the buoyant fluid offshore of the shelfbreak current velocity maximum forms the streamer. The destination of the buoyant water contained in the streamer is identified by the maximum offshore displacement of the streamer $D_{\max}/R_c$, which is shown in Fig. 10. For experiments with $\epsilon \leq 1$, the streamer is only slightly deflected offshore, with $D_{\max}/R_c$ ranging from 2.9 when $\epsilon = 0.28$ to 7.5 when $\epsilon \approx 1$. During weak interactions, the offshore transport is small (about 20% or less of the geostrophic transport at the shelf break) and varies little with ϵ (Fig. 11).

b. *Strong interactions* ($\epsilon > 1$)

When the self-propagating anticyclonic vortex comes into contact with the shelfbreak current, the outermost fluid in the shelfbreak current is pulled offshore by the vortex to form a streamer (Fig. 8b, blue trajectories). The buoyant fluid forming the streamer is not observed to reconnect with the shelfbreak current downstream of the region of interaction, resulting in a permanent loss of fluid from the shelf to the slope. The outermost vortex fluid is engulfed by the shelfbreak current as in the weak interaction regime (Fig. 8b, red trajectories). The vortex fluid again spools off the vortex, but during a strong interaction the time scale for spooling is much longer

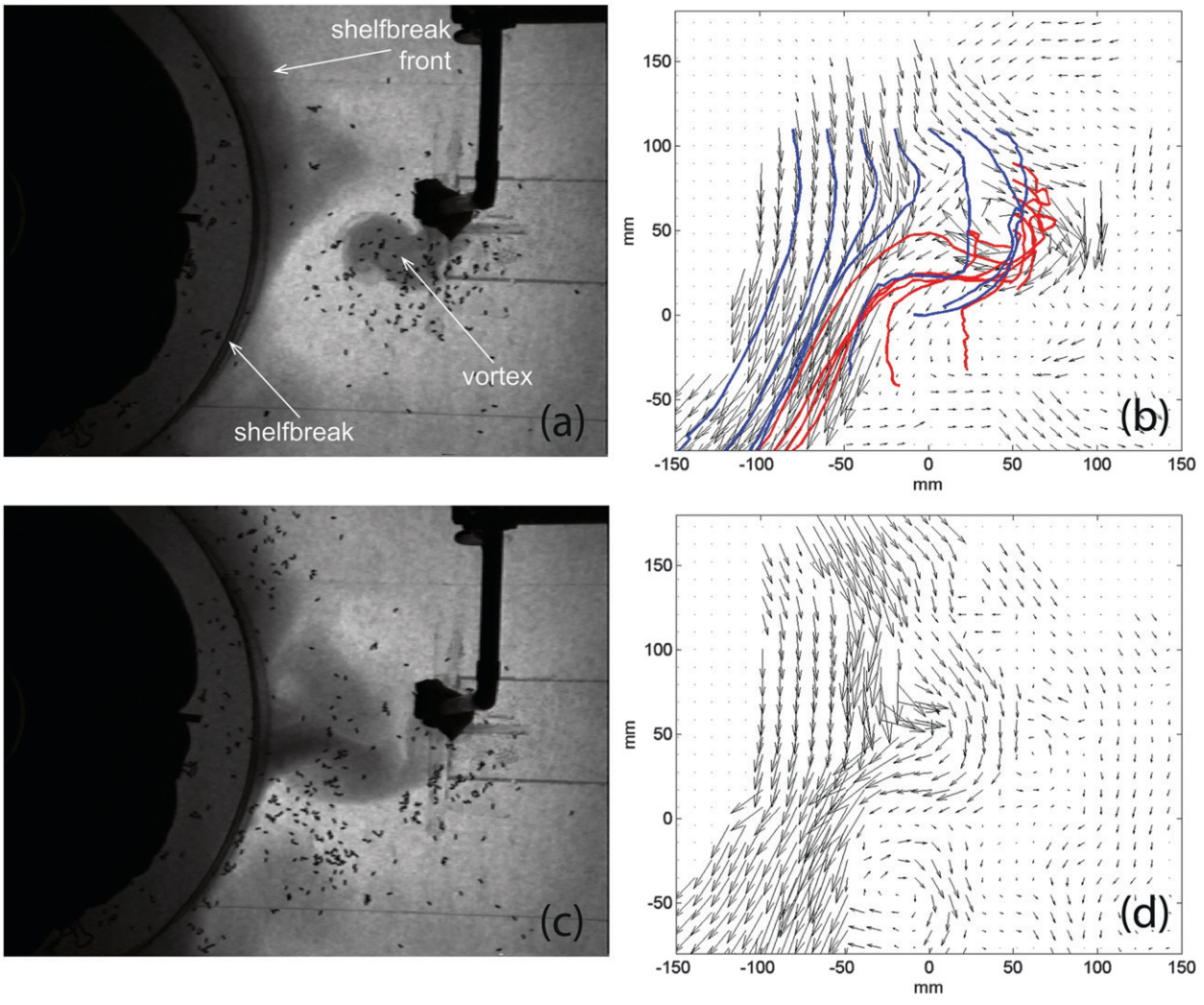

FIG. 7. Snapshots of a weak interaction ($\epsilon = 0.37$). The vortex water is engulfed by the shelfbreak current, which is deflected slightly offshore before moving back over the shelfbreak downstream of the interaction region. Top view images and velocity fields at (a),(b) $1.3T$ and (c),(d) $4.1T$, where T is the rotation period, and $t = 0$ when the anticyclonic vortex generation is completed. (a),(c) The darker gray represents the shelfbreak current water and the lighter gray the vortex water. Blue (red) lines in (b) show the trajectories of synthetic drifters released in the current (vortex) at $t = 1.3T$.

and the vortex is able to permanently deflect part of the buoyant shelf water offshore in a streamer. Furthermore, part of the vortex fluid is able to penetrate onto the shelf (Fig. 8b, red trajectories).

The fraction of the shelfbreak current that is deflected onto the slope increases for increasing values of ϵ (Fig. 9). The largest values of $d_{\max}/R_c$ are measured for the experiments presenting the strongest interaction (i.e., the largest values of ϵ). For two experiments, the value of $d_{\max}/R_c$ is negative, indicating that only the fluid offshore of the shelfbreak current velocity maximum forms the streamer. This scenario occurs for values of ϵ near unity, the transition between the strong and weak regimes. The largest offshore displacement of the streamer $D_{\max}/R_c = 16$ is obtained for $\epsilon = 2.11$, the largest value of ϵ in the laboratory (Fig. 10); hence, the fluid within the streamer is less likely to reconnect with the shelfbreak current when $\epsilon > 1$ than in cases with $\epsilon < 1$ in which the streamer is only slightly deflected offshore.

For $\epsilon > 1$, the offshore transport by streamers increases with increasing ϵ (Fig. 11). For the largest values of ϵ the offshore transport exceeds the geostrophic transport of the shelfbreak current (i.e., $T_s/Q > 1$) and, as expected when looking at the values of $d_{\max}/R_c$, the offshore transport includes buoyant water inshore of the shelfbreak current velocity maximum. Streamer transports are as much as 170% of the geostrophic transport of the shelfbreak current; offshore transport exceeding

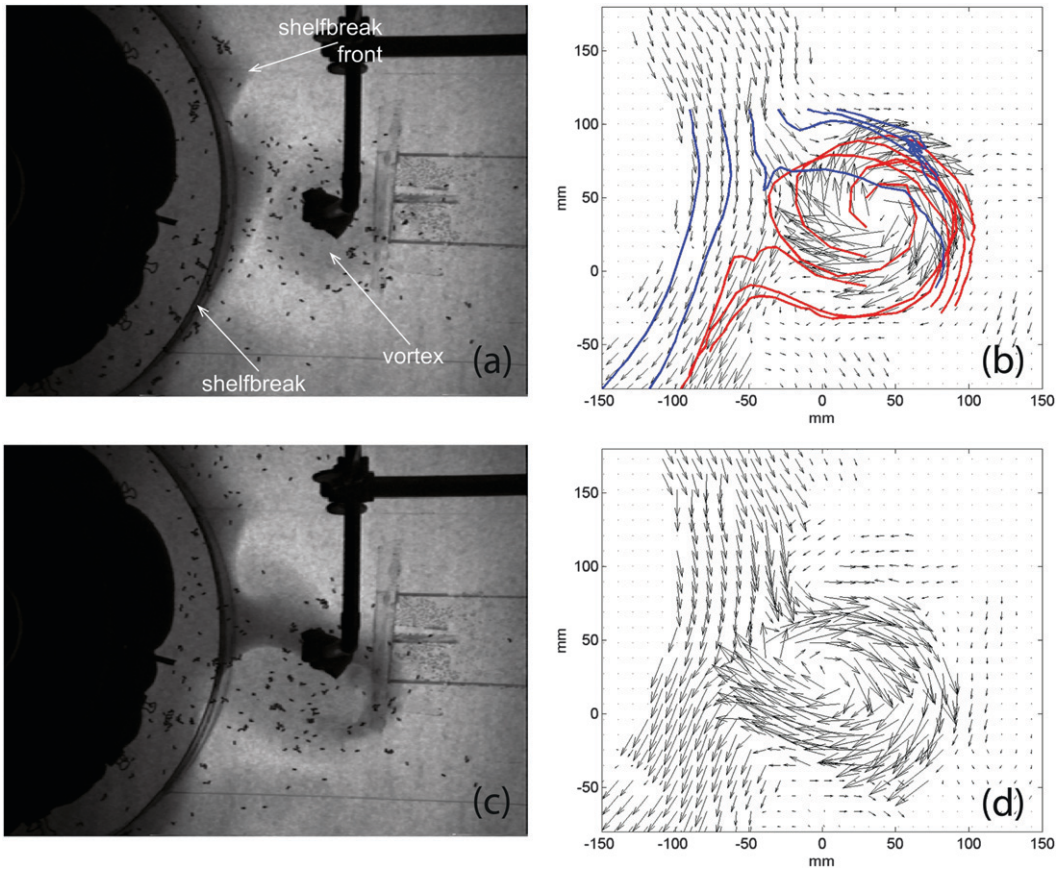

FIG. 8. As in Fig. 7, but for a strong interaction ($\epsilon = 2.07$). Part of the shelfbreak current is deflected offshore as a streamer in (c) and the fluid within the streamer does not reconnect with the shelfbreak current downstream, causing a permanent loss of fluid from the shelf to the offshore. Top-view images and velocity fields at (a),(b) $0.6T$ and (c),(d) $2.9T$. Blue (red) lines in (b) show the trajectories of synthetic drifters released in the current (vortex) at $t = 0.6T$.

the transport of the shelfbreak current must include waters from the shelf where buoyant waters have near zero velocities prior to the vortex interaction. These waters are carried far offshore of the shelf break resulting in permanent exchange.

c. *Comparison to MAB observations*

The observations of vortex–current interactions in the MAB from 2005, 2006, and 2007 span the range of values of ϵ produced in the laboratory. The two vortices observed in the MAB in spring 2006 and summer 2007 (Fig. 1) are representative of the strong and weak interactions observed in the laboratory, respectively. In the spring of 2006, the maximum vertically averaged velocity measured by the glider was 1.32 m s^{-1} on the eastern side of the vortex; the shipboard ADCP found a peak current velocity of 1.95 m s^{-1} at 25-m depth on the western side of the vortex (Table 2). Since vertically averaged currents underestimate peak velocities, we take the 1.95 m s^{-1} measurement as representative of the vortex velocity; this measurement compares favorably with the 1.7 m s^{-1} velocity reported for the same WCR in the numerical simulations of Chen (2011). The azimuthal velocity of the smaller vortex during summer 2007 was substantially lower, with a maximum velocity of 0.48 m s^{-1} found at 20-m depth along the glider transect through the middle of the vortex (Fig. 6a). However, the shelfbreak current velocities were comparable between spring 2006 and summer 2007 with peak westward velocities of 0.45 and 0.55 m s^{-1}, respectively (Table 2). The shelfbreak current velocities are somewhat higher than those reported in climatologies (e.g., Linder and Gawarkiewicz 1998) since the climatologies smooth over meanders of the shelfbreak current. Resulting estimates of ϵ for the MAB vortices in spring 2006 and summer 2007 are 4.33 and 0.86, respectively. Based on the laboratory results, we expect that the vortex in spring 2006 strongly affected the shelfbreak current, while the vortex during the summer of 2007 interacted weakly with the shelfbreak current.

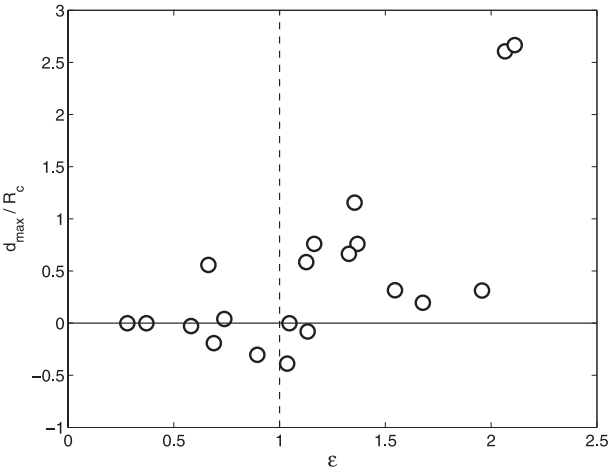

FIG. 9. Measured values of $d_{\max}/R_c$ for the laboratory experiments spanning a range of values of ϵ. The dashed line at $\epsilon = 1$ denotes the transition between strong and weak interactions.

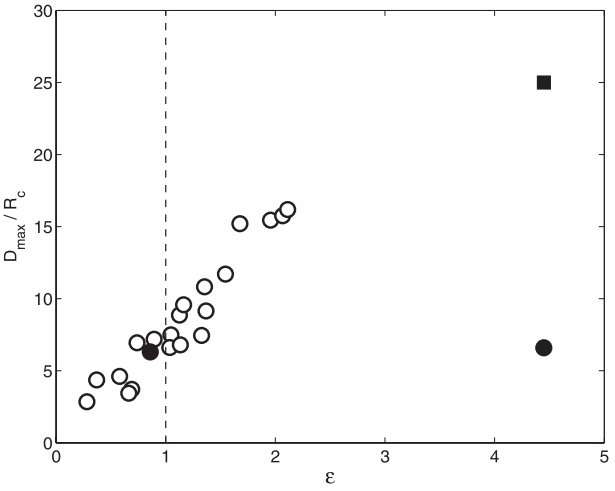

FIG. 10. Observations of maximum offshore extent of shelf water, $D_{\max}/R_c$, as a function of ϵ for laboratory experiments (open symbols) and MAB observations (solid symbols). For the 2006 WCR observations with $\epsilon = 4.33$, two values of $D_{\max}/R_c$ are shown, with the square denoting the SST-derived estimate and the circle indicating the value estimated from in situ observations.

In addition to the vastly different azimuthal velocities, the spring 2006 and summer 2007 vortices differ in their vertical extent (Table 2). High salinity waters of Gulf Stream origin penetrated to a depth of at least 680 m within the 2006 WCR, while salinities greater than 36.0 g kg^{-1} were confined to the upper 250 m in the weaker vortex of summer 2007. Estimates of g'_v are similar for the two vortices, so the depth of the features is the primary contributor to the larger Rossby radius R_v for the 2006 WCR compared to the vortex of summer 2007. The difference in estimated Rossby radii for the two vortices is also consistent with the difference in size of the vortices, as is apparent in SST images (Figs. 1b,c).

As expected from the laboratory results, the large WCR in spring 2006 had significant impacts on the shelfbreak current in the MAB. A streamer of cold, fresh shelf water formed along the eastern side of the vortex and was apparent in both SST imagery (Fig. 1b) and the glider observations (Fig. 5). Shelf water with salinity less than 34.9 g kg^{-1} was found as far south as 39.4°N (approximately 70 km from the shelf break) in the glider observations, yielding an estimate of $D_{\max}/R_c \approx 6.6$ (Table 2). This estimate, which is substantially lower than expected from the laboratory experiments (Fig. 10), is an underestimate since the glider moved from the perimeter of the WCR into the interior of the WCR near that latitude (Fig. 5). In the SST imagery (Fig. 1b), cool shelf waters are drawn out to the northern edge of the Gulf Stream near 37.7°N (approximately 250 km from the shelf break), resulting in $D_{\max}/R_c \approx 25$, in better agreement with an extrapolation of the laboratory results. Averaging the results from the two methods described in section 2b, T_s/Q was about 2.9, indicating that large amounts of buoyant shelf water were drawn offshore as the WCR interacted with the shelfbreak front. Chen (2011) reported mean cross-frontal transport during April–May 2006 that equaled the climatological mean transport of the shelfbreak current ($T_s/Q \approx 1$) and instantaneous streamer transports as much as seven times greater near the WCR. The large streamer transport ($T_s/Q \gg 1$) inferred for the WCR is consistent with the laboratory finding that T_s/Q grows with ϵ for $\epsilon > 1$ (Fig. 11).

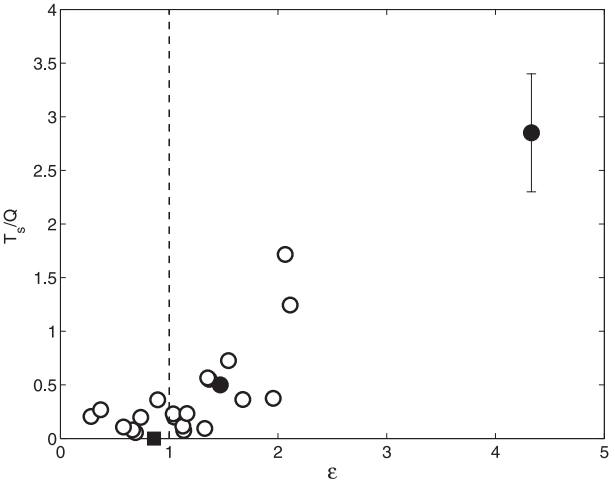

FIG. 11. Streamer transport as a fraction of the geostrophic transport in the shelfbreak current T_s/Q plotted against ϵ for laboratory experiments (open symbols) and MAB observations (solid symbols). The solid square represents the suggestion of weak or absent offshore transport for the smaller anticyclonic vortex in the summer 2007 (i.e., $T_s/Q \approx 0$) as discussed in section 3c. The bars for the MAB observation at $\epsilon = 4.33$ indicate the range of estimates for T_s/Q (Table 2) and the symbol indicates the average value.

The smaller anticyclonic vortex in the summer of 2007 had a weaker impact on the shelfbreak current, consistent with the laboratory findings for $\epsilon < 1$. On the eastern side of the vortex, the farthest offshore extent of shelf water in the glider observations was 39.1°N along the north–south transect (Fig. 6b; $D_{max}/R_c \approx 6.3$, Table 2). Cross-track geostrophic currents were eastward near 39°N (Fig. 6b), so it seems that shelf water was only found on the northern side of the vortex and had not wrapped around the perimeter of the vortex. Neither SST imagery nor vertically averaged currents suggest significant offshore transport because of a streamer on the eastern side of the vortex. Both the estimate of $D_{max}/R_c \approx 6.3$ and the suggestion of weak or absent offshore transport ($T_s/Q \approx 0$, solid square in Fig. 11) are in good agreement with the laboratory results (Figs. 10 and 11).

The streamer measured by the AUV in July 2005 falls into an intermediate case with a value of $\epsilon = 1.47$ and a ratio of the streamer transport to the geostrophic transport of the shelfbreak current $T_s/Q \approx 0.5$. For this observation, the size of the baroclinic Rossby radius over the shelf was 5.3 km. While we do not have estimates of the slope vortex scales or density structure, the cross-frontal transport is consistent with the relationship obtained from the laboratory experiments (Fig. 11).

4. Summary and conclusions

Laboratory experiments are carried out to investigate the interaction between a baroclinic anticyclonic vortex and a shelfbreak current. The behavior of the interaction is studied while varying a key parameter, the ratio ϵ of the maximum azimuthal velocity in the vortex to the maximum alongshelf velocity in the shelfbreak current. For large values of ϵ the interaction is strong and a streamer of shelf water detaches from the shelfbreak current and wraps around the anticyclonic vortex. The water in the streamer originates inshore of the shelfbreak current maximum velocity (i.e., $d_{max}/R_c > 0$) and is carried offshore several Rossby radii of deformation, with a consequent offshore transport of shelf waters that can reach up to 170% of the shelfbreak current geostrophic transport. Furthermore, for strong interactions, some of the vortex waters move over the shelf and are entrained into the shelfbreak current. As ϵ decreases, the vortex is less effective at transporting shelf waters offshore. For $\epsilon < 1$, the shelfbreak current engulfs the vortex, and some shelf waters are slightly deflected offshore before reconnecting with the shelfbreak front. Only the waters located around or offshore of the shelfbreak current maximum velocity interact with the vortex (i.e., $d_{max}/R_c \leq 0$) and the offshore transport is limited to $\lesssim$20% of the geostrophic transport of the shelfbreak current. A significant difference between the weak and the strong interactions is the fate of the water transported offshore. For the smallest values of ϵ, the water forming the streamer reconnects with the shelfbreak current, while, for the largest values of ϵ, the streamer is deflected offshore far enough (up to $D_{max}/R_c = 16$) that it remains offshore and does not return to the shelf.

Values of the parameter ϵ for anticyclonic vortices interacting with the MAB shelfbreak current range from 0.86 to 4.33 (Table 2). Quantitative estimates of the offshore transport by streamers and the offshore displacement of shelf waters for three very different values of ϵ, indicative of weak, strong, and intermediate interactions, are in good agreement with the laboratory model prediction. The range of values of ϵ for anticyclonic vortices interacting with the MAB shelfbreak current suggests that a variety of different types of cross-frontal exchanges can occur in this region. For an accurate estimate of the offshore transport of shelf waters through the mechanism described in this study, it is necessary to have a probability distribution of the values of ϵ in the MAB, but a statistical analysis of the strength (i.e., v_v) of the anticyclonic vortices compared to the strength (i.e., v_c) of the shelfbreak current is still missing. The present work suggests that such an analysis should be conducted to allow reliable estimates of the cross-frontal exchange of heat, salt, carbon, nutrients, sediments, and other water characteristics due to anticyclonic vortices interacting with the shelfbreak front.

Acknowledgments. We thank Gianluca Cesarei for analyzing some of the laboratory data. The laboratory experiments were carried out with the able assistance of Keith Bradley. Laboratory work was supported by the National Science Foundation through Grant OCE-0081756. Glider observations in March–April 2006 were supported by the National Science Foundation through Grant OCE-0220769. Glider observations in July–October 2007 were supported by a grant from Raytheon. RET was supported by the Postdoctoral Scholar Program at the Woods Hole Oceanographic Institution, with funding provided by the Cooperative Institute for the North Atlantic Region. The REMUS observations were funded by the Office of Naval Research. GGG was supported by the National Science Foundation through Grant OCE-1129125 for analysis and writing.

APPENDIX

Cyclonic Vortex–Current Interaction

The results described above pertain to an anticyclonic baroclinic vortex interacting with a shelfbreak current.

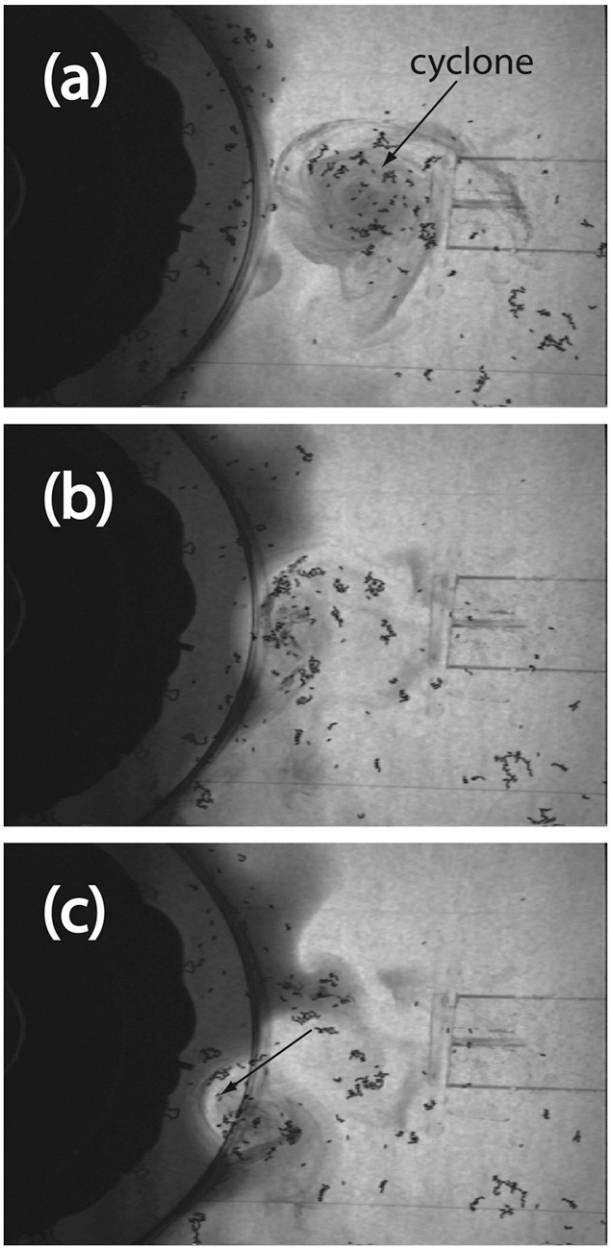

FIG. A1. Cyclonic barotropic vortex interaction with a buoyant coastal current. (a) Just prior to interaction at $t = 11.3T$; (b) the cyclone squeezes the current inshore over the shelf at $t = 17.7T$; and (c) part of the cyclone's water moves over the shelf at $t = 19.1T$ as indicated by the arrow, where T is the rotation period and $t = 0$ when the cyclonic vortex generation is completed. For this experiment $f = 1.5\ s^{-1}$, $g_c' = 1.6\ cm\ s^{-2}$, and $h_c = 1.5$ cm.

Although perhaps less relevant to an oceanic application, a few experiments were performed to qualitatively examine the interaction between a cyclonic barotropic vortex and a shelfbreak current. The cyclonic vortex is generated in the tank by placing an ice cube in the water (Whitehead et al. 1990; Cenedese 2002), a method dynamically similar to withdrawing fluid from a sink positioned on the sloping bottom. Because of conduction, the water surrounding the ice cube becomes colder than the surrounding water and sinks as a cold plume, forming a cold, dense lens within the thin bottom Ekman layer. The cold, dense plume entrains ambient water inducing inward velocities in the water column above the bottom lens that, influenced by the Coriolis force, generate a cyclonic vortex. The vortex is influenced by the presence of the sloping bottom and self-propagates westward with a very small meridional displacement.

When the barotropic cyclonic vortex reaches the shelfbreak current, the vortex ''squeezes'' the current over the shelf as some of its fluid moves over the shelf (Fig. A1b). The fluid within the shelfbreak current where the velocity is maximum is subsequently deflected inshore in the vicinity of the cyclonic vortex, and then it moves back onto the shelfbreak downstream of the interaction. As time progresses, more fluid from the cyclonic vortex moves over the shelf, as shown by the arrow in Fig. A1c, while the core of the vortex remains just off the shelf break. However, a streamer of buoyant shelf water is not observed to form and be deflected offshore as in the case of an anticyclonic baroclinic vortex.

REFERENCES

Bisagni, J. J., 1983: Lagrangian current measurements within the eastern margin of a warm-core Gulf Stream ring. *J. Phys. Oceanogr.,* **13,** 709–715.

Bogazzi, E., and Coauthors, 2005: Spatial correspondence between areas of concentration of Patagonian scallop (*Zygochlamys patagonica*) and frontal systems in the southwestern Atlantic. *Fish. Oceanogr.,* **14,** 359–376, doi:10.1111/j.1365-2419.2005.00340.x.

Brink, K., R. Limeburner, and R. Beardsley, 2003: Properties of flow and pressure over Georges Bank as observed with near-surface drifters. *J. Geophys. Res.,* **108,** 8001, doi:10.1029/2001JC001019.

Cenedese, C., 2002: Laboratory experiments on mesoscale vortices colliding with a seamount. *J. Geophys. Res.,* **107** (C6), doi:10.1029/2000JC000599.

——, and P. Linden, 1999: Cyclone and anticyclone formation in a rotating stratified fluid over a sloping bottom. *J. Fluid Mech.,* **381,** 199–223.

——, and J. Whitehead, 2000: Eddy-shedding from a boundary current around a cape over a sloping bottom. *J. Phys. Oceanogr.,* **30,** 1514–1531.

——, and P. Linden, 2002: The stability of a buoyancy-driven coastal current at the shelf break. *J. Fluid Mech.,* **452,** 97–121.

Chaudhuri, A. H., J. J. Bisagni, and A. Gangopadhyay, 2009: Shelf water entrainment by Gulf Stream warm-core rings between 75°W and 50°W during 1978–1999. *Cont. Shelf Res.,* **29,** 393–406, doi:10.1016/j.csr.2008.10.001.

Chen, K., 2011: Middle Atlantic Bight shelfbreak circulation dynamics and biophysical interactions. Ph.D. thesis, North Carolina State University, 169 pp.

Churchill, J. H., P. C. Cornillon, and G. W. Milkowski, 1986: A cyclonic eddy and shelf-slope water exchange associated with

a Gulf Stream warm-core ring. *J. Geophys. Res.,* **91** (C8), 9615–9623.

Coachman, L. K., 1986: Circulation, water masses, and fluxes on the southeastern Bering Sea shelf. *Cont. Shelf Res.,* **5** (1–2), 23–108, doi:10.1016/0278-4343(86)90011-7.

Dalziel, S. B., 1992: *DigImage: System Overview*. Cambridge Environmental Research Consultants, 43 pp.

Evans, R. H., K. S. Baker, O. B. Brown, and R. C. Smith, 1985: Chronolgy of warm-core ring 82B. *J. Geophys. Res.,* **90** (C5), 8803–8811.

Flierl, G., and J. Wroblewski, 1985: The possible influence of warm core Gulf Stream rings upon the shelf water larval fish distribution. *Fish. Bull.,* **83,** 313–330.

Garfield, N., III, and D. L. Evans, 1987: Shelf water entrainment by Gulf Stream warm-core rings. *J. Geophys. Res.,* **92** (C12), 13 003–13 012.

Gawarkiewicz, G. G., and D. C. Chapman, 1992: The role of stratification in the formation and maintenance of shelf-break fronts. *J. Phys. Oceanogr.,* **22,** 753–772.

——, F. Bahr, R. C. Beardsley, and K. H. Brink, 2001: Interaction of a slope eddy with the shelfbreak front in the Middle Atlantic Bight. *J. Phys. Oceanogr.,* **31,** 2783–2796.

Griffiths, R., and P. Linden, 1981: The stability of buoyancy-driven coastal currents. *Dyn. Atmos. Oceans,* **5,** 281–306.

Intergovernmental Oceanographic Commission, 2010: The international thermodynamic equation of seawater–2010: Calculation and use of thermodynamic properties. Intergovernmental Oceanographic Commission Manuals and Guides No. 56, 196 pp.

Joyce, T. M., J. K. B. Bishop, and O. B. Brown, 1992: Observations of offshore shelf-water transport induced by a warm-core ring. *Deep Sea Res. Part A,* **39** (Suppl. 1), S97–S113.

Linden, P., B. Boubnov, and S. Dalziel, 1995: Source-sink turbulence in a rotating stratified fluid. *J. Fluid Mech.,* **298,** 81–112.

Linder, C. A., and G. G. Gawarkiewicz, 1998: A climatology of the shelfbreak front in the Middle Atlantic Bight. *J. Geophys. Res.,* **103** (C9), 18 404–18 423.

Loder, J. W., B. Petrie, and G. G. Gawarkiewicz, 1998: The coastal ocean off northeastern North America: A large-scale view. *The Sea: The Global Coastal Ocean,* A. R. Robinson and K. H. Brink, Eds., *Regional Studies and Syntheses,* Vol. 11, Wiley, 105–133.

Marra, J., R. W. Houghton, and C. Garside, 1990: Phytoplankton growth at the shelf-break front in the Middle Atlantic Bight. *J. Mar. Res.,* **48,** 851–868.

Morgan, C. W., and J. M. Bishop, 1977: An example of Gulf Stream eddy-induced water exchange in the Mid-Atlantic Bight. *J. Phys. Oceanogr.,* **7,** 472–479.

Nof, D., 1983: The translation of isolated cold eddies on a sloping bottom. *Deep-Sea Res.,* **30,** 171–182.

Oguz, T., and Coauthors, 1993: Circulation in the surface and intermediate layers of the Black Sea. *Deep-Sea Res. I,* **40,** 1597–1612, doi:10.1016/0967-0637(93)90018-X.

Orphanides, C. D., and G. M. Magnusson, 2007: Characterization of the northeast and Mid-Atlantic Bottom and Mid-Water Trawl Fisheries based on Vessel Trip Report (VTR) data. National Oceanic and Atmospheric Association, Northeast Fisheries Science Center Ref. Doc. 07-15, 140 pp.

Peña-Molino, B., T. M. Joyce, and J. M. Toole, 2013: Variability in the Deep Western Boundary Current: Local versus remote forcing. *J. Geophys. Res.,* **117,** C12022, doi:10.1029/2012JC008369.

Pingree, R. D., G. T. Mardell, P. M. Holligan, D. K. Griffiths, and J. Smithers, 1982: Celtic Sea and Armorican current structure and the vertical distributions of temperature and chlorophyll. *Cont. Shelf Res.,* **1,** 99–116, doi:10.1016/0278-4343(82)90033-4.

Rudnick, D. L., R. E. Davis, C. C. Eriksen, D. M. Fratantoni, and M. J. Perry, 2004: Underwater gliders for ocean research. *Mar. Technol. Soc. J.,* **38,** 73–84.

Shearman, R. K., and S. J. Lentz, 2004: Observations of tidal variability on the New England shelf. *J. Geophys. Res.,* **109,** C06010, doi:10.1029/2003JC001972.

Sherman, J., R. E. Davis, W. B. Owens, and J. Valdes, 2001: The autonomous underwater glider ''Spray.'' *IEEE J. Oceanic Eng.,* **26,** 437–446.

Smith, P. C., 1978: Low-frequency fluxes of momentum, heat, salt, and nutrients at the edge of the Scotian Shelf. *J. Geophys. Res.,* **83** (C8), 4079–4096.

Springer, A. M., C. P. McRoy, and M. V. Flint, 1996: The Bering Sea Green Belt: Shelf-edge processes and ecosystem production. *Fish. Oceanogr.,* **5** (3/4), 205–223, doi:10.1111/j.1365-2419.1996.tb00118.x.

Tang, C. L., A. S. Bennett, and D. J. Lawrence, 1985: Thermohaline intrusions in the frontal zones of a warm-core ring observed by Batfish. *J. Geophys. Res.,* **90** (C5), 8928–8942.

Todd, R. E., D. L. Rudnick, M. R. Mazloff, R. E. Davis, and B. D. Cornuelle, 2011: Poleward flows in the southern California Current System: Glider observations and numerical simulation. *J. Geophys. Res.,* **116,** C02026, doi:10.1029/2010JC006536.

——, G. G. Gawarkiewicz, and W. B. Owens, 2013: Horizontal scales of variability over the Middle Atlantic Bight shelf break and continental rise from finescale observations. *J. Phys. Oceanogr.,* **43,** 222–230.

Toole, J. M., R. G. Curry, T. M. Joyce, M. McCartney, and B. Peña Molino, 2011: Transport of the North Atlantic Deep Western Boundary Current about 39°N, 70°W: 2004–2008. *Deep-Sea Res. II,* **58,** 1768–1780, doi:10.1016/j.dsr2.2010.10.058.

Wei, J., D.-P. Wang, and C. N. Flagg, 2008: The interaction of an vortex with an unstable jet. *J. Geophys. Res.,* **113,** C10021, doi:10.1029/2007JC004694.

Whitehead, J. A., M. E. Stern, G. R. Flierl, and B. A. Klinger, 1990: Experimental observations of baroclinic eddies on a sloping bottom. *J. Geophys. Res.,* **95** (C6), 9585–9610.

Wright, W. R., and C. E. Parker, 1976: A volumetric temperature/salinity census for the Middle Atlantic Bight. *Limnol. Oceanogr.,* **21,** 563–571.